IOP Publishing Bioinspir. Biomim. 19 (2024) 036010 https://doi.org/10.1088/1748-3190/ad3601

Bioinspiration & Biomimetics

PAPER

S-shaped rolling gait designed using curve transformations of a snake robot for climbing on a bifurcated pipe

Jingwen Lu[1], Chaoquan Tang[1,*], Eryi Hu[2] and Zhipeng Li[1]

[1] School of Mechatronic Engineering, China University of Mining and Technology, Xuzhou, People's Republic of China
[2] Information Institute, Ministry of Emergency Management of the People's Republic of China, Beijing, People's Republic of China
[*] Author to whom any correspondence should be addressed.

E-mail: tangchaoquan@cumt.edu.cn

RECEIVED
12 November 2023

REVISED
21 February 2024

ACCEPTED FOR PUBLICATION
20 March 2024

PUBLISHED
2 April 2024

Keywords: snake robot, hyper-redundant mechanism, biologically-inspired robots, motion control, gait design

Abstract

In this work, we focus on overcoming the challenge of a snake robot climbing on the outside of a bifurcated pipe. Inspired by the climbing postures of biological snakes, we propose an S-shaped rolling gait designed using curve transformations. For this gait, the snake robot's body presenting an S-shaped curve is wrapped mainly around one side of the pipe, which leaves space for the fork of the pipe. To overcome the difficulty in constructing and clarifying the S-shaped curve, we present a method for establishing the transformation between a plane curve and a 3D curve on a cylindrical surface. Therefore, we can intuitively design the curve in 3D space, while analytically calculating the geometric properties of the curve in simple planar coordinate systems. The effectiveness of the proposed gait is verified by actual experiments. In successful configuration scenarios, the snake robot could stably climb on the pipe and efficiently cross or climb to the bifurcation while maintaining its target shape.

1. Introduction

A snake robot is a redundant mechanism consisting of many joints connected in series, and it is capable of multiple forms of motion. Hirose and Yamada [1] successfully demonstrated the world's first serpentine motion by using a snake robot composed of parallel joints in 1972, and promoted the development of snake robots with 3D motion capabilities. Lipkin *et al* [2] achieved a helical rolling gait for the first time to enable a snake robot to climb the outside of a pipe. Pipe climbing, such as used for checking or repairing, is a typical and unique 3D task for snake robots. However, interconnected pipes in facilities can form bifurcations that hinder the climbing of snake robots with a conventional helical rolling gait as shown in figure 1.

Researchers have tried to find effective solutions to overcome the challenge of a snake robot climbing a bifurcated pipe. Kuwada *et al* [3] proposed a method for adapting to changes in pipe shapes through joint force feedback. Rollinson and Choset [4] used a compliance controller to direct a snake robot to automatically adapt to the shape of the fork, but this method can only be used for climbing inside pipes. [5–7] proposed methods for achieving climbing motion along curved pipes by designing target curves. However, the solution strategies mentioned in [3–7] can be applied only to climbing inside pipes. The *helical wave propagation motion* proposed by Qi *et al* [8, 9] has the ability to cross the bifurcation, but it uses stop-and-go movements with low propulsion speed on the outside of the pipe. Nakajima *et al* [10] proposed a *spiral stairs function* to surpass a branch by shifting and rolling motions at the local contact point between the snake robot and the pipe. Although the snake robot can cross the branch faster when more body parts are detached from the pipe, the friction between the snake robot and the pipe is reduced, preventing the *spiral stairs function* from being used on a vertical pipe. Takemori *et al* [11] used adaptive helical rolling to enable snake robots to climb a pipe with an irregular cross-sectional shape due to its bifurcation. However, the distance of this motion at the fork was limited, and the snake robot could not completely pass through the bifurcation.

The bifurcation that a snake robot has to overcome on the outside of a pipe is distinct from changes

Figure 1. The forked pipes cannot be handled with a conventional helical rolling gait. (a) Interconnected pipes in facilities. (b) The helical rolling motion cannot pass through the forked pipe.

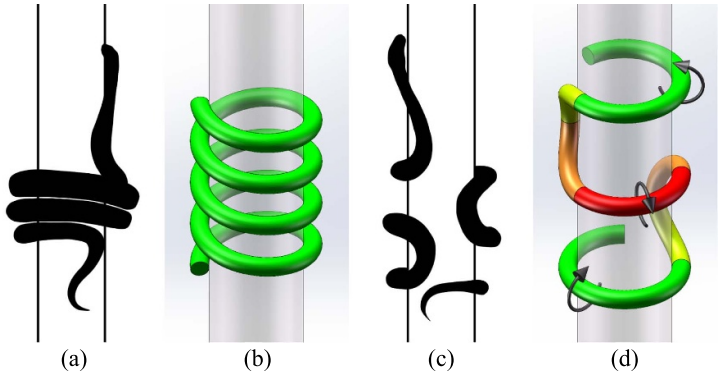

Figure 2. Two forms of biological snakes wrapping their bodies around cylinders. (a) A biological snake that wraps around a pipe in a helical form. (b) Helical curve. (c) A biological snake that wraps around a pipe in an S-shaped form. (d) S-shaped curve. Arrows represent the directions of the corresponding parts when the S-shaped curve rolls.

in the diameter or shape of pipes [11–13], since the bifurcation is equivalent to an infinitely extending obstacle. The postures of biological snakes climbing pipes provide a reference for overcoming this challenge in mechanical snakes. Biological snakes usually wrap their bodies around pipes in a helix or an S-shape as shown in figure 2, and then stretch their bodies to climb based on these two forms [14–17]. In addition, the S-shaped form of movement requires the body to be wrapped around only one side of the pipe, providing space for the bifurcation. Tang and Shu *et al* [18, 19] proposed *Planar-cylindrical gaits transformation mechanism* and used this method to implement climbing gaits based on the S-shaped form. However, they did not conduct detailed studies or experimental verifications of the obstacle avoidance capability for the gait, and the planning processes in the plane were too tedious to facilitate adjustments of the gait during use. Takemori *et al* [20–23] proposed a method for designing the form of a snake robot by connecting simple shapes, which greatly improved the convenience and practicability of gait design with curves. However, only three simple curves with constant curvature and torsion can be used, which limits the design of gaits to some extent. Konishi *et al* [24] used connecting curve segments to design a climbing gait with an S-shaped posture, but using only simple curves could not construct S-shaped curves that fit a pipe, resulting in the gait that could not run on a vertical pipe and could only span a small bifurcation. In addition, a large frictional force was generated between the snake robot and the pipe during morphological transformations, which was likely to cause the morphology to deviate from desired targets or even collapse.

In contrast, mechanical snakes have difficulty achieving smooth stretching motions like biological snakes due to the long distance between their joints, but their bodies are not divided into a back and abdomen, making climbing more efficient with rolling motions. Therefore, we were committed to applying the S-shaped rolling motion to the pipe climbing of snake robots, and more importantly, to equip them with the ability to cross or climb to the bifurcation. The generation of our proposed S-shaped rolling gait is based on using the curvature and torsion of a curve

Table 1. Performance comparisons between related work and the gait form proposed in this paper.

Work	Cross the bifurcation		Climb to the bifurcation		Others
	The trunk	Time taken	The trunk	Time taken	
Qi *et al* [9]	Vertical	Approximately 180 s			
Nakajima *et al* [10]	Horizontal	Unknown			
Konishi *et al* [24]	Inclined	Approximately 60 s			Easy to deform
This paper	Horizontal and vertical	Approximately 40 s	Horizontal	Approximately 47 s	

and twist angles between the curve segments to obtain the angles of the snake robot's joints [20, 25]. To address the difficulty in constructing and clarifying the S-shaped curve, we propose a method to transform between a planar curve and a 3D curve on a cylindrical surface, in which the 3D curve is regarded as formed by wrapping the planar curve onto a cylinder. Therefore, we can intuitively design the curve in 3D space, and analytically calculate the geometric properties of the curve in a simple plane coordinate system. The gait proposed in this paper has the following technical advantages when dealing with climbing on the outside of forked pipes:

(1) Using curve transformation to design the target shape of gait can make the snake robot fit pipes better and reduce the risk of falling from pipes.
(2) This gait has two functions, crossing or climbing to the bifurcation. In particular, studies on climbing from the trunk to the bifurcation outside the pipe are lacking.
(3) The curvatures of the curve segments corresponding to the head and tail of the snake robot are alternately transformed to switch shapes. The shape transformation does not cause sliding friction between the snake robot and the pipe, allowing for better maintenance of the target shape.
(4) The shape transformation and rolling motion can be carried out simultaneously, without the need to pause the rolling motion used for propulsion, ensuring the propulsion speed of the snake robot on the pipe.

The following are comparisons between related works and this paper. The solutions mentioned in [3–7] can be applied only to climbing inside the pipe. The interconnected pipes do not hinder the snake robot inside them, and the main problem in this case is steering. For a snake robot climbing outside a pipe, dealing with the bifurcation involves not only steering, but also obstacle avoidance. Therefore, detailed comparisons are made here on the physical experiments of snake robots climbing the outside of forked pipes. Table 1 shows the performance comparisons between the relevant studies and the proposed motion forms in this paper. Due to the influence of gravity, the conditions for snake robots to climb on a vertical pipe are stricter than those on a horizontal pipe, with the inclined pipe being between the two. The corresponding time for related work comes from the paper or accompanying video. The video attached to [24] shows multiple experimental projects, and the table shows the shortest time it takes for most of the snake robot's body to pass through the bifurcation. Although the experimental results were influenced by the physical parameters of the snake robot and the pipes, these parameters were checked and there was no large difference between them. It can be clearly concluded from the table that our proposed gait form has significant advantages in terms of applicable scenarios, propulsion speed, and stability. In addition, to our knowledge, there is a lack of research on how a snake robot climbs from the trunk to the bifurcation outside the pipes in the published work where physical experiments were conducted.

The rest of this paper is organized as follows: section 2 describes the method to establish the transformation between a plane curve and a 3D curve on a cylindrical surface for constructing and clarifying the S-shaped curve. Section 3 describes the design of the S-shaped rolling gait. In section 4, we demonstrate the effectiveness of the gait experimentally. Finally, section 5 concludes this paper.

2. Transformation of curves

2.1. Wrapping a plane curve around the cylinder

A smooth curve C_2 in a plane coordinate system, is shown in figure 3. The coordinate of any point on the curve C_2 can be expressed with the parameter t as $(x(t), y(t))$. The parameter value corresponding to the starting point of the curve is t_0.

As shown in figure 4, the coordinate of any point $P(X, Y, Z)$ on the cylindrical surface in the 3D rectangular coordinate system O_XYZ can be expressed as follows:

$$\begin{cases} X = R\cos\theta + X_0 \\ Y = R\sin\theta + Y_0 \\ Z = h \end{cases} \tag{1}$$

where R is the radius of the cylinder, X_0 and Y_0 are the horizontal and vertical coordinates, respectively, projected by the axis of the cylinder on the plane XOY, θ is the phase angle of point P on the cylindrical surface, and h is the distance from point P to plane XOY.

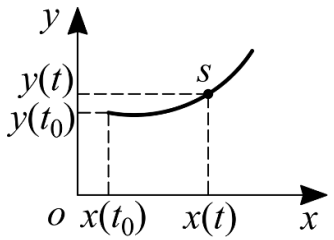

Figure 3. Curve C_2 in a plane coordinate system.

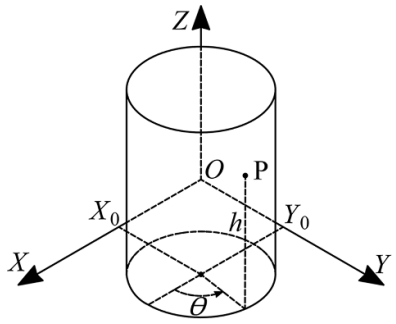

Figure 4. A point on the cylindrical surface in the 3D rectangular coordinate system.

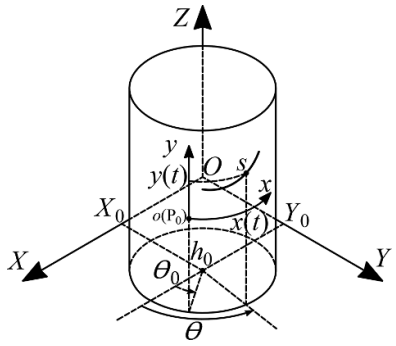

Figure 5. Transformation of the plane curve to a wrapped curve on the cylindrical surface.

As shown in figure 5, if we wrap the plane coordinate system with the above curve C_2 onto the cylindrical surface, we can obtain a 3D curve C_3, which is later called the 'wrapped curve'. In figure 4, the origin o of the plane coordinate system and P_0 on the cylindrical surface in the 3D coordinate system coincide, and the positive directions of the axis y of the plane coordinate system and the axis Z of the 3D coordinate system are the same, thus, the parameters θ and h in (1) can be expressed as:

$$\begin{cases} \theta = \frac{x(t)}{R} + \theta_0 \\ h = y(t) + h_0 \end{cases} \tag{2}$$

where θ_0 and h_0 are the parameter values corresponding to the point P_0. By substituting (2) into (1), the parametric equation of the wrapped curve C_3 can P_0 be written as follows:

$$\begin{cases} X(t) = R\cos\left[\dfrac{x(t)}{R} + \theta_0\right] + X_0 \\ Y(t) = R\sin\left[\dfrac{x(t)}{R} + \theta_0\right] + Y_0 \\ Z(t) = y(t) + h_0 \end{cases}. \tag{3}$$

Thus far, we have expressed the wrapped curve C_3 in 3D space with the parameter t defined in the planar coordinate system, which enables us to study the properties of the curve C_3 through the curve C_2. The first derivative of (3) with respect to the parameter t can be obtained as follows:

$$\begin{cases} X'(t) = -x'(t)\cdot\sin\left[\dfrac{x(t)}{R} + \theta_0\right] \\ Y'(t) = x'(t)\cdot\cos\left[\dfrac{x(t)}{R} + \theta_0\right] \\ Z'(t) = y'(t) \end{cases}. \tag{4}$$

According to the operation of the elementary functions, when the plane curve C_2 is smooth in the interval $[t_1, t_2]$, the wrapped curve C_3 is also smooth in the same interval.

The formulas for solving the curvature and torsion of the 3D curve with respect to parameter t are as follows:

$$\begin{cases} \kappa(t) = \dfrac{\sqrt{(Y'Z'' - Z'Y'')^2 + (Z'X'' - X'Z'')^2 + (X'Y'' - Y'X'')^2}}{\left[(X')^2 + (Y')^2 + (Z')^2\right]^{\frac{3}{2}}} \\ \tau(t) = \dfrac{X^{(3)}(Y'Z'' - Z'Y'') + Y^{(3)}(Z'X'' - X'Z'') + Z^3(X'Y'' - Y'X'')}{(Y'Z'' - Z'Y'')^2 + (Z'X'' - X'Z'')^2 + (X'Y'' - Y'X'')^2} \end{cases} \tag{5}$$

By continuing the derivation of (4) with respect to t, the second and third derivatives of X, Y and Z can be obtained as follows:

$$\begin{cases} X'' = -\frac{1}{R}\cos\left(\frac{x}{R}+\theta_0\right)\cdot(x')^2 - \sin\left(\frac{x}{R}+\theta_0\right)\cdot x'' \\ Y'' = -\frac{1}{R}\sin\left(\frac{x}{R}+\theta_0\right)\cdot(x')^2 + \cos\left(\frac{x}{R}+\theta_0\right)\cdot x'' \\ Z'' = y'' \end{cases} \tag{6}$$

$$\begin{cases} X^{(3)} = \sin\left(\frac{x}{R}+\theta_0\right)\cdot\left[\frac{1}{R}(x')^3 - x^{(3)}\right] - \frac{3}{R}\cos\left(\frac{x}{R}+\theta_0\right)\cdot x'x'' \\ Y^{(3)} = -\cos\left(\frac{x}{R}+\theta_0\right)\cdot\left[\frac{1}{R}(x')^3 - x^{(3)}\right] - \frac{3}{R}\sin\left(\frac{x}{R}+\theta_0\right)\cdot x'x'' \\ Z^{(3)} = y^{(3)} \end{cases} \tag{7}$$

By substituting (4), (6) and (7) into (5) and simplifying, the curvature and torsion of the wrapped curve C_3 with respect to t can be obtained as follows:

$$\begin{cases} \kappa(t) = \dfrac{\sqrt{(x'y''-x''y')^2 + \frac{1}{R^2}(x')^4\left[(x')^2+(y')^2\right]}}{\left[(x')^2+(y')^2\right]^{\frac{3}{2}}} \\ \tau(t) = \dfrac{(x')^2y'\left[\frac{1}{R^2}(x')^3 - x^{(3)}\right] - 3x'x''(x'y''-y'x'') + (x')^3y^{(3)}}{R(x'y''-x''y')^2 + \frac{1}{R}(x')^4\left[(x')^2+(y')^2\right]} \end{cases} \tag{8}$$

From (8), it can be found that the curvature $\kappa(t)$ and the torsion $\tau(t)$ of the wrapped curve C_3 are independent of the values of X_0, Y_0, θ_0, h_0, x and y, and are related only to the first, second and third derivatives of x and y with respect to the parameter t. In other words, the curvature and torsion of a curve are geometric properties related to the shape of the curve, that can be described using the coordinate system, but do not depend on the coordinate system selection. Therefore, when solving for the curvature and torsion, we can set the coordinate system at a convenient location for calculation.

In the planar coordinate system, when parameter t changes from the initial value t_0, the corresponding length s can be expressed as:

$$s(t) = \pm\int_{t_0}^{t}\sqrt{\left[x'(\hat{t})\right]^2 + \left[y'(\hat{t})\right]^2}\,\mathrm{d}\hat{t} \tag{9}$$

where $\pm$ is determined by the change in parameter t, which is a positive sign when parameter t changes in the positive direction; otherwise, it is a negative sign.

The function $t(s)$ of t with respect to s can be obtained by solving the inverse function of (9). Since the lengths s of the plane curve and the wrapped curve are identical with respect to the parameter t, the curvature $\kappa(s)$ and torsion $\tau(s)$ of the wrapped curve C_3 with respect to s are obtained by substituting the function $t(s)$ into (8). Then, $\kappa(s)$ and $\tau(s)$ can be used to calculate the angles of a snake robot's joints [25].

2.2. The plane curves satisfying the condition

Only when the function of the length s of the plane curve with respect to the parameter t has an inverse, can $\kappa(t)$ and $\tau(t)$ convert to $\kappa(s)$ and $\tau(s)$. A few plane curves, including the vertical line, the horizontal line, the diagonal line and the circular arc, meet this condition. Fortunately, these four curves can 'extend, twine and turn' on the cylinder after being wrapped, and their combination is sufficient to construct an S-shaped curve.

In figure 6, from left to right, a vertical line, a horizontal line, a diagonal line and a circular arc on the planar coordinate systems, which are wrapped onto the cylindrical surface to form a straight line, a circular arc, a helix and an arc-like curve close to the cylinder, are shown. The expressions of these four plane curves, as well as the curvatures and torsions formed by wrapping them on the cylinder, are given in table 2, where a is the abscissa of the point where the vertical line intersects the axis x, b and c are the ordinates of the points where the horizontal line and the diagonal line intersect the axis y, k is the slope of the diagonal

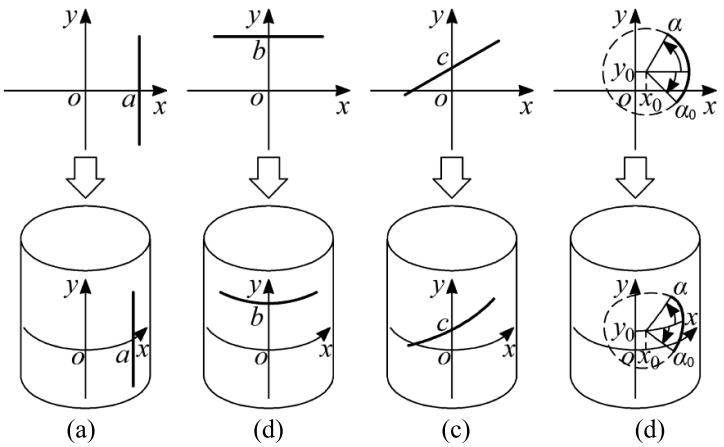

Figure 6. Four plane curves satisfying the condition. (a) Vertical line. (b) Horizontal line. (c) Diagonal line. (d) Circular arc.

Table 2. The four plane curves satisfying the condition and the curvatures and torsions of the wrapped curves on the cylinder.

Plane curve	$\kappa(s)$ and $\tau(s)$ of wrapped curve
Vertical line: $x=a$	$\kappa(s)=0\ \tau(s)=0$
Horizontal line: $y=b$	$\kappa(s)=1/R\ \tau(s)=0$
Diagonal line:$y=kx+c$	$\kappa(s)=1/\left[R\left(1+k^2\right)\right]\ \tau(s)=k/\left[R\left(1+k^2\right)\right]$
Circular arc: $\begin{cases} x=r\cos\alpha+x_0 \\ y=r\sin\alpha+y_0 \end{cases}$	$\kappa(s)=\sqrt{1/(r^2)+1/(R^2)\sin^4[\alpha(s)]}$
	$\tau(s)=\dfrac{\left(\frac{r}{R}\right)^2\sin^5[\alpha(s)]\cos[\alpha(s)]+\frac{3}{2}\sin 2[\alpha(s)]}{-R-\frac{r^2}{R}\sin^4[\alpha(s)]}$
	$\alpha(s)=\pm\dfrac{s}{r}+\alpha_0$

line, r is the radius of the circular arc, α is the phase angle of the point on the circular arc, α_0 is the phase angle corresponding to the starting point of the circular arc, and (x_0,y_0) is the coordinate of the center of the circular arc.

In the following, we refer to the curve formed by wrapping the circular arc as the 'wrapped arc'. For simplicity, the curvature and torsion of the wrapped arc are denoted as $\kappa_{\mathrm{wa}}(R,r,\alpha(s))$ and $\tau_{\mathrm{wa}}(R,r,\alpha(s))$.

In addition, cycloids and involutes also meet the conditions, and readers can deduce according to the above method.

2.3. Twist angle of a connection point

When a smooth curve is formed by splicing multiple curve segments, twist angles need to be attached to connection points [20]. However, if the curvatures or torsions of the curve segments are not constant, the twist angles at the connection points cannot be obtained through an exclusive geometric calculation. We similarly apply this idea of reducing the dimension to address the problem by processing function equations of the plane curves to determine the twist angle at the connection point of the 3D curve.

Within each curve segment, the binormal unit vector $e_{\mathrm{B}}(t)$ and the tangential unit vector $e_{\mathrm{T}}(t)$ can be obtained as follows:

$$\boldsymbol{e}_{\mathrm{B}}(t)=\pm\frac{\left(Y'Z''-Z'Y'',Z'X''-X'Z'',X'Y''-Y'X''\right)}{\sqrt{(Y'Z''-Z'Y'')^2+(Z'X''-X'Z'')^2+(X'Y''-Y'X'')^2}} \tag{10}$$

$$\boldsymbol{e}_{\mathrm{T}}(t)=\pm\frac{\left(X',Y',Z'\right)}{\sqrt{(X')^2+(Y')^2+(Z')^2}} \tag{11}$$

where $\pm$ is determined by the change in parameter t, which is a positive sign when parameter t changes in the positive direction; otherwise, it is a negative sign.

The twist angle between the left limit $\boldsymbol{e}_{\mathrm{B}}\left(s_j^-\right)$ and the right limit $\boldsymbol{e}_{\mathrm{B}}\left(s_j^+\right)$ of the binormal unit vector at the connection point s_j can be obtained as:

$$\psi_j=\pm\arccos\left[\boldsymbol{e}_{\mathrm{B}}\left(t_j^-\right)\cdot\boldsymbol{e}_{\mathrm{B}}\left(t_j^+\right)\right] \tag{12}$$

where j is the index of a connection point and t_j^- and t_j^+ are the parameters corresponding to s_j^- and s_j^+, respectively. Since s_j^- and s_j^+ are located in different curve segments, the meanings of t_j^- and t_j^+ may be different in terms of their plane coordinates, and the value range of $|\psi_j|$ is $[0,\pi]$. As shown in figure 7, the sign of the directed angle ψ_j can be judged by the right-hand rule.

The directed angle ψ_j can also be obtained as:

$$\psi_j=\mathrm{sign}\left[\boldsymbol{e}_{\mathrm{B}}\left(t_j^-\right)\times\boldsymbol{e}_{\mathrm{B}}\left(t_j^+\right)\cdot\boldsymbol{e}_{\mathrm{T}}\left(t_j^\pm\right)\right]\cdot|\psi_j| \tag{13}$$

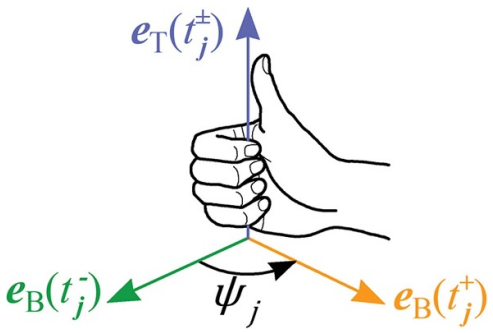

Figure 7. Judging the sign of ψ_j by the right-hand rule, the sign of ψ_j is positive in this case.

The twist angle ψ_j is also a geometric property of the curve itself, and does not depend on the selection of coordinate systems. Therefore, when we solve for ψ_j, we can equally set the coordinate systems in a convenient position for calculation.

3. Gait design

3.1. S-shaped curve

As shown in figure 1(b), when the body of a biological snake is wrapped on a pipe with an S-shape, all parts of it contact the pipe. If a machine snake rolls in this form, the middle loop (red) and the loops at the two ends (green) will be opposite to the direction of friction between the pipe, and the whole body will slip on the pipe and not produce effective movement.

As shown in figure 8, to prevent the machine snake from slipping when rolling in an S-shape, the middle loop is reset to be separated from the pipe. The entire S-shaped curve is composed of multiple segments. Segments 1, 2, 8 and 9 are circular arcs and segments 3 and 7 are wrapped arcs, which are wrapped around a cylindrical surface with radius R_1 and contact with the pipe. Segments 4 and 6 are wrapped arcs around a cylindrical surface with radius R_2, and segment 5 is a circular arc around a cylindrical surface with radius R_3; none of these segments contact the pipe. The planes of all the circular arcs are perpendicular to the axis of the pipe. The distinction of segments 1 and 9 from segments 2 and 8 is to address the bifurcation while climbing.

In figure 8, O_{13} is the intersection point between the axis of the cylindrical surfaces with radii R_1 and R_3 and the bottom surface, and O_2 is the intersection point between the axis of the cylindrical surface with radius R_2 and the bottom surface. A, B and C are the connection points between segments 2 and 3, 3 and 4, and 4 and 5, respectively. BH is the vertical line of $O_{13}C$. The four points O_{13}, O_2, A and C lie on the same line. Figure 9 shows the S-shaped curve expanded into a plane, where s_0 is the starting point of the curve and s_j is the connection point between segment j and segment $j+1$. In the plane, segments 3 and 7 are circular arcs with radius r_1, and segments 4 and 6 are circular arcs with radius r_2. R_1 is determined by the diameter of the pipe D_p and the diameter of the snake D_s:

$$R_1 = \frac{(D_\mathrm{p}+D_\mathrm{s})}{2} \tag{14}$$

R_3 can be expressed as follows:

$$R_3 = R_1 + d \tag{15}$$

where d is the clearance between segment 5 and the pipe. d and r_1 are set by the operator. R_2 and r_2 can be obtained:

$$\mathrm{BH} = \mathrm{BO}_{13} \cdot \sin\left(\frac{\overset{\frown}{AB}}{R_1}\right) = R_1 \cdot \sin\left(\frac{r_1}{R_1}\right) \tag{16}$$

$$\mathrm{HC} = \mathrm{O}_{13}\mathrm{C} - \mathrm{O}_{13}\mathrm{H} = R_3 - R_1 \cdot \cos\left(\frac{r_1}{R_1}\right) \tag{17}$$

$$\angle \mathrm{BO}_2\mathrm{C} = \pi - 2\angle \mathrm{O}_2\mathrm{CB} = \pi - 2\arctan\left(\frac{\mathrm{BH}}{\mathrm{HC}}\right) \tag{18}$$

$$R_2 = \mathrm{BO}_2 = \frac{\mathrm{BH}}{\sin \angle \mathrm{BO}_2\mathrm{C}} \tag{19}$$

$$r_2 = \overset{\frown}{BC} = R_2 \cdot \angle \mathrm{BO}_2\mathrm{C}. \tag{20}$$

The radians of segments 4, 6 and 7 in the plane are $\pi/2$, and they maintain the same lengths in 3D space. The sum of the lengths of all curve segments equals the length of the snake robot's body:

$$\sum_{j=1}^{9} l_j = (n+1) \cdot l \tag{21}$$

where l_j is the length of segment j, n is the total number of the snake robot's joints, and l is the distance between adjacent joints of the snake robot.

3.2. Calculating the curvatures, torsions and twist angles

As shown in figure 9, segments 1, 2, 5, 8 and 9 are horizontal lines in the coordinate system $x_1o_1y_1$. We obtain the curvatures of segments 1, 2, 8 and 9 as $1/R_1$ and the curvature of segment 5 as $1/R_3$ in 3D space, with torsions of 0. In the coordinate system $x_2o_2y_2$, segment 3 is a circular arc whose starting point s_2 corresponds to the phase angle $-\pi/2$. When we use s_0 as the starting point, the curvature and torsion of segment 3 can be written as follows:

$$\begin{cases} \kappa_3(s) = \kappa_{\mathrm{wa}}\left(R_1, r_1, \frac{s-s_2}{r_1} - \frac{\pi}{2}\right) \\ \tau_3(s) = \tau_{\mathrm{wa}}\left(R_1, r_1, \frac{s-s_2}{r_1} - \frac{\pi}{2}\right) \end{cases}. \tag{22}$$

The curvatures and torsions of segments 4, 6 and 7 in 3D space can be obtained similarly and are given in table 3.

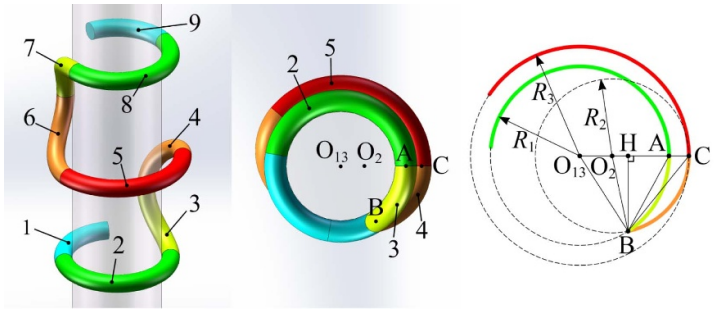

Figure 8. S-shaped curve for the machine snake's rolling gait. (a) Stereoscopic view. (b) View parallel to the axis of the pipe. (c) Simplification of the curve in (b).

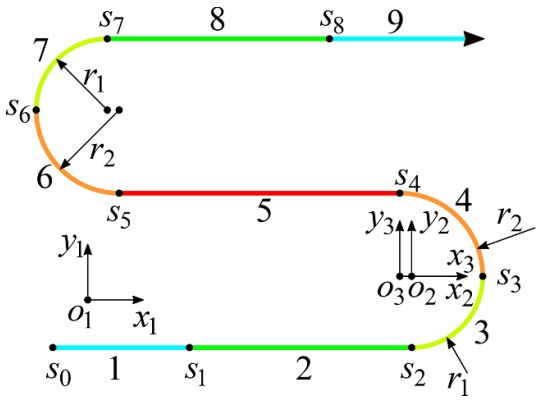

Figure 9. S-shaped curve in the plane.

Table 3. Curvature and torsion of each segment forming the S-shaped curve in 3D space and the twist angle of the connection point.

Index j	Curvature $\kappa_j(s)$	Torsion $\tau_j(s)$	Twist angle ψ_j
1	$1/R_1$	0	0
2	$1/R_1$	0	$\arccos\frac{r_1}{\sqrt{R_1^2+r_1^2}}$
3	$\kappa_{wa}\left(R_1, r_1, \frac{s-s_2}{r_1}-\frac{\pi}{2}\right)$	$\tau_{wa}\left(R_1, r_1, \frac{s-s_2}{r_1}-\frac{\pi}{2}\right)$	$\left\lvert\frac{r_1}{R_1}-\frac{r_2}{R_2}\right\rvert$
4	$\kappa_{wa}\left(R_2, r_2, \frac{s-s_3}{r_2}\right)$	$\tau_{wa}\left(R_2, r_2, \frac{s-s_3}{r_2}\right)$	$-\arccos\frac{r_2}{\sqrt{R_2^2+r_2^2}}$
5	$1/R_3$	0	$-\arccos\frac{r_2}{\sqrt{R_2^2+r_2^2}}$
6	$\kappa_{wa}\left(R_2, r_2, \frac{s_5-s}{r_2}-\frac{\pi}{2}\right)$	$\tau_{wa}\left(R_2, r_2, \frac{s_5-s}{r_2}-\frac{\pi}{2}\right)$	$\left\lvert\frac{r_1}{R_1}-\frac{r_2}{R_2}\right\rvert$
7	$\kappa_{wa}\left(R_1, r_1, \frac{s_6-s}{r_1}+\pi\right)$	$\tau_{wa}\left(R_1, r_1, \frac{s_6-s}{r_1}+\pi\right)$	$\arccos\frac{r_1}{\sqrt{R_1^2+r_1^2}}$
8	$1/R_1$	0	0
9	$1/R_1$	0	—

As shown in figure 10, a 3D rectangular coordinate system O_XYZ is established. The axis Z coincides with the axis of the cylindrical surface with radius R_1, the plane XOY passes through point s_3, and the plane XOZ passes through points s_2 and s_4. Combining the established planar coordinate systems $x_2o_2y_2$ and $x_3o_3y_3$, the left and right limit binormal unit vectors and tangent unit vectors of point s_3 in the 3D coordinate system O_XYZ can be obtained as follows:

$$\begin{cases} \boldsymbol{e}_B\left(t_3^-\right) = \left(\cos\left(\frac{r_1}{R_1}\right), \sin\left(\frac{r_1}{R_1}\right), 0\right) \\ \boldsymbol{e}_B\left(t_3^+\right) = \left(\cos\left(\frac{r_2}{R_2}\right), \sin\left(\frac{r_2}{R_2}\right), 0\right) \\ \boldsymbol{e}_T\left(t_3^\pm\right) = (0,0,1) \end{cases} \tag{23}$$

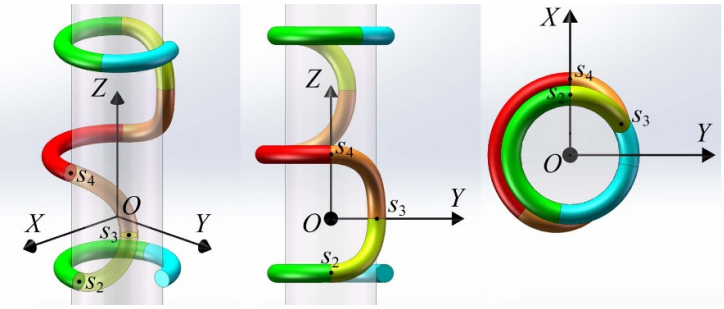

Figure 10. The 3D coordinate system for calculating ψ_3. (a) Stereoscopic view. (b) The view is normal to the plane *YOZ*. (c) The view is normal to the plane *XOY*.

The twist angles of the connection point s_3 can be obtained as follows:

$$\psi_3 = \left| \frac{r_1}{R_1} - \frac{r_2}{R_2} \right| . \tag{24}$$

Although the cylindrical surfaces covered by segments 3 and 4 are different, the left and right limit tangent unit vectors $e_T\left(t_3^-\right)$ and $e_T\left(t_3^+\right)$ at the connection point s_3 are equal. Therefore, the S-shaped curve in 3D space is still smooth at point s_3. Similarly, there are points s_4, s_5, and s_6.

The twist angles of other connection points can be obtained equivalently, and their values are given in table 3.

The angles of the snake robot's joints fitting the '*backbone curve*' can be obtained by using the curvatures, torsions and twist angles [20, 25]. For the snake robot with orthogonal joints, the angles of each joint fitting the S-shaped curve in 3D space can be calculated as follows:

$$\theta_i = \begin{cases} \int_{(i-1)l}^{(i+1)l} -\kappa(s)\sin\psi(s)\,\mathrm{d}s & (i:\text{odd}) \\ \int_{(i-1)l}^{(i+1)l} \kappa(s)\cos\psi(s)\,\mathrm{d}s & (i:\text{even}) \end{cases} \tag{25}$$

$$\psi(s) = \psi_0 + \int_0^s \tau(\hat{s})\,\mathrm{d}\hat{s} + \sum_{j=1}^{m} \psi_j \tag{26}$$

where i is the index of a joint, m is the number of connection points in the length of s, ψ_0 is an arbitrary integration constant, and the entire snake robot produces a rolling motion by changing ψ_0 with time. In addition, we adopted an optimized coding method [26] to reduce the computational load of the computer and improve the fluency of the gait operation in the experiments.

Since joint angles are limited by the maximum $\theta_{\max}$, the curvature $\kappa(s)$ must meet the following condition:

$$|\theta_i| = \begin{cases} \left| \int_{s_t+(i-1)l}^{s_t+(i+1)l} -\kappa(s)\sin\psi(s)\,\mathrm{d}s \right| & (i:\text{odd}) \\ \left| \int_{s_t+(i-1)l}^{s_t+(i+1)l} \kappa(s)\cos\psi(s)\,\mathrm{d}s \right| & (i:\text{even}) \end{cases}$$

$$\leqslant \left| \int_{s_t+(i-1)l}^{s_t+(i+1)l} \kappa(s)\,\mathrm{d}s \right| \leqslant \int_{s_t+(i-1)l}^{s_t+(i+1)l} \kappa_{\max}\mathrm{d}s = 2l\kappa_{\max} \leqslant \theta_{\max} \tag{27}$$

where $\kappa_{\max}$ is the maximum value of the curvature $\kappa(s)$ in the integration interval. This can provide reference ranges for the values of curve parameters. However, the curvature in the integration interval may not always be the maximum value, so this is a sufficient and unnecessary condition.

3.3. Overcoming bifurcation in climbing

As shown in figure 11, if the snake robot must cross a bifurcation while climbing, it should align the 'notched' side of its S-shaped body with the bifurcation. When the head is about to reach the bifurcation, we reverse segment 9 by changing its curvature to a negative value. After the upper loop has passed the bifurcation, segment 9 is recovered. We control segment 1 in the same way until the lower loop passes the bifurcation. Throughout the process, at least one of the head and tail of the snake robot is tightly wrapped around the pipe to ensure stability and provide sufficient power. When using shift motions along a backbone curve to avoid obstacles, sliding friction occurs between the snake robot and the pipe, which in turn led to deformation or even collapse of the snake robot's body shape [24]. This drawback does not exist in the form transformation by changing signs of the curvatures of segments 1 and 9.

In addition, considering the stability of the snake robot on the pipe and dealing with bifurcation, some key points need to be noted when setting the lengths of segments 2, 5, and 8. If the trunk is vertical, the modules of the snake robot should wrap around the pipe at least half a circle to ensure the force balance of the snake robot [27]. As shown in figure 12, segment 9

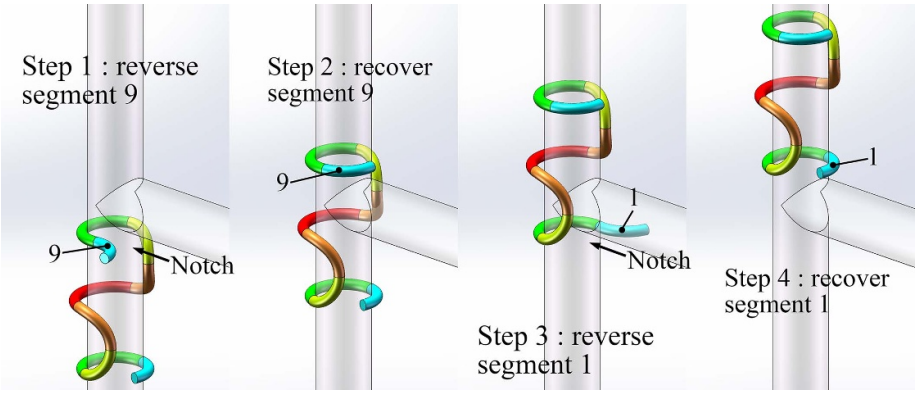

Figure 11. Key control steps in the process of crossing a bifurcation.

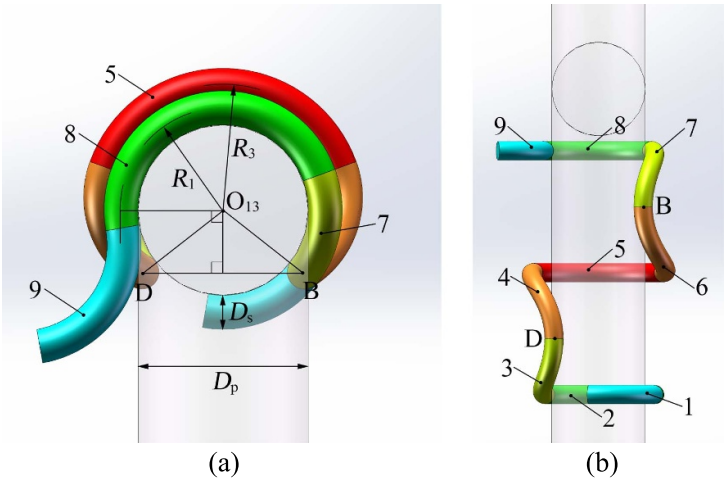

Figure 12. Schematic diagram for setting parameters l_5, l_2 and l_8. (a) The view is parallel to the trunk's axis. (b) The view is parallel to the axis of the bifurcation.

will detach from the pipe as it approaches the bifurcation, at which point this end relies on segments 7 and 8 for stability. The projection of segments 7 and 8 on a plane perpendicular to the axis of the trunk is a circular arc, and the corresponding central angle of this arc must satisfy the following relationship:

$$\frac{l_8 + r_1}{R_1} \geqslant \pi \tag{28}$$

Similarly, the length of segment 2 must meet the same condition. Setting the length of each segment of the S-shaped curve symmetrically, the values of the lengths of segments 2 and 8 must meet:

$$l_2 = l_8 \geqslant \pi R_1 - r_1 \ . \tag{29}$$

The S-shaped curve also needs to be configured with enough space to pass through the bifurcation. The projection of the point s_6 on the plane perpendicular to the trunk's axis is denoted as D, and the chord length BD can be expressed as follows:

$$\mathrm{BD} = 2R_1 \cdot \sin\left[\frac{1}{2}\left(2\pi - \frac{l_5}{R_3} - 2\frac{r_1}{R_1}\right)\right] \ . \tag{30}$$

In the experiments of this paper, the diameter of the bifurcation is the same as that of the trunk, so the theoretical chord length BD needs to meet:

$$\mathrm{BD} \geqslant D_\mathrm{p} + D_\mathrm{s} \ . \tag{31}$$

By substituting (30) into (31), the length of segment 5 needs to meet the following requirement:

$$l_5 \leqslant 2R_3\left(\frac{\pi}{2} - \frac{r_1}{R_1}\right) \ . \tag{32}$$

To prevent interference with the bifurcation after the 9 segments detach from the trunk, the theoretical length of the 8 segments needs to meet:

$$\frac{l_8}{R_1} \leqslant 2\pi - \frac{r_1}{R_1} - \frac{\pi}{2} - \frac{1}{2}\left(2\pi - \frac{l_5}{R_3} - 2\frac{r_1}{R_1}\right) \ . \tag{33}$$

Therefore, the length of segments 2 and 8 still needs to meet:

$$l_2 = l_8 \leqslant R_1\left(\frac{\pi}{2} + \frac{l_5}{2R_3}\right) \ . \tag{34}$$

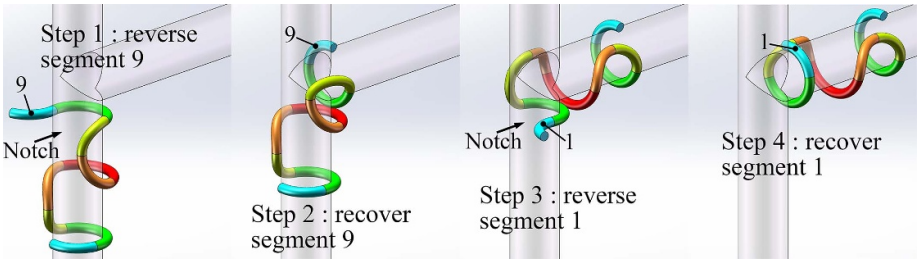

Figure 13. Key control steps in the process of climbing to a bifurcation.

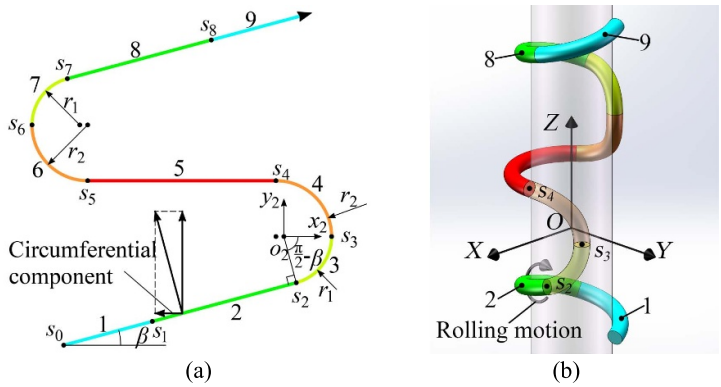

Figure 14. The S-shaped curve for circumferential rotation and adjustment. (a) The curve in the plane. (b) The curve in 3D space.

The actual values of l_5, l_2 and l_8 can be slightly greater than the upper limits given by (32) and (34), and the interference between the snake robot and the pipe can be adapted due to the limited joint torque.

The S-shaped rolling gait essentially uses the same process to climb to the bifurcation. As shown in figure 13, if the snake robot must climb from the trunk to the bifurcation, it aligns the 'notch' side of its body with the bifurcation in reverse. The climbing direction of the snake robot at the fork will be limited. Because the position control mode of each actuator is within its torque limit, the angle of each joint may not reach the target value, allowing the snake robot to produce compliant motion and adapt to the shape of the fork.

3.4. Circumferential rotation and adjustment

As shown in figure 14, we change segments 1, 2, 8 and 9 of the planar S-shaped curve to diagonal lines with an inclination β, resulting in helixes wrapped in 3D space. The component of rolling displacement along the circumferential direction adjusts the relative position of the notch to the bifurcation. As needed, the snake robot can adjust its position by climbing back and forth within a range on the pipe.

As the shape of the curve changes, the radians of segments 3 and 7 are replaced by $\pi/2-\beta$ in the plane. The slopes of segments 1, 2, 8 and 9 are all $\tan\beta$, The curvatures and torsions of their corresponding helices can be obtained from table 2. Because the phase angle corresponding to the starting point s_2 of segment 3 in the coordinate system $x_2o_2y_2$ becomes $-(\pi/2-\beta)$, $-\pi/2$ should be replaced by $-(\pi/2-\beta)$ in (22).

The left and right limit binormal unit vectors at point s_2 are replaced by:

$$\boldsymbol{e}_{\mathrm{B}}\left(t_2^-\right)=\sin\beta\left(\sin\left(\frac{r_1\sin\beta}{R_1}\right),\cos\left(\frac{r_1\sin\beta}{R_1}\right),\cot\beta\right) \tag{35}$$

$$\boldsymbol{e}_{\mathrm{B}}\left(t_2^+\right)=\frac{1}{\sqrt{1+\left(\frac{r_1}{R_1}\cos^2\beta\right)^2}}\begin{bmatrix}\cos\left(\frac{r_1\sin\beta}{R_1}\right)+\frac{r_1}{R_1}\sin\left(\frac{r_1\sin\beta}{R_1}\right)\cos^2\beta\sin\beta\\ \sin\left(\frac{r_1\sin\beta}{R_1}\right)-\frac{r_1}{R_1}\cos\left(\frac{r_1\sin\beta}{R_1}\right)\cos^2\beta\sin\beta\\ \frac{r_1}{R_1}\cos^3\beta\end{bmatrix}^{\mathrm{T}}. \tag{36}$$

Then the twist angles ψ_2 and $\psi_7$can be recalculated with (35) and (36).

4. Experiment

We used a physical snake robot to verify the effectiveness of the proposed S-shaped rolling gait for climbing on the outside of a bifurcated pipe. Figure 15 shows our experimental equipment. The snake robot we used is composed of alternating pitch and yaw joints. The number of joints is 37, the range of each

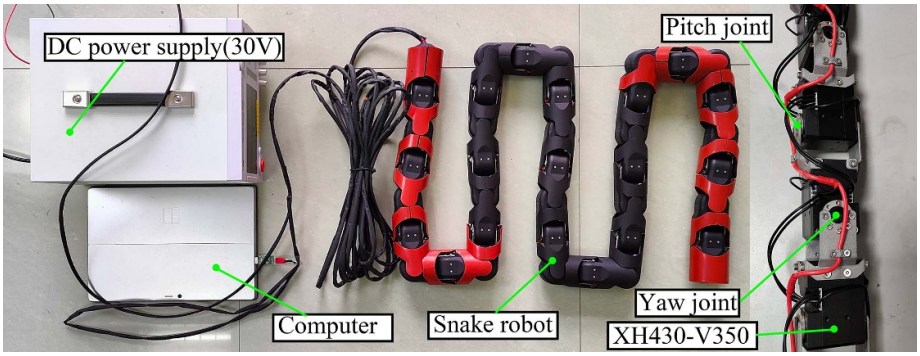

Figure 15. Our experimental equipment. On the right side of the figure are the joints and actuators exposed after the snake robot's housing is removed.

joint is $\pm 90°$, and the distance between adjacent joints is 60 mm. Each module approximately has a diameter of 54 mm and a mass of 115 g. The actuator of each joint is a DYNAMIXEL XH430-V350 with a maximum torque of 4 Nm. All the actuators are powered by a 30 V DC, and the target angle of each joint is sent from the computer following the RS-485 protocol. Because the S-shaped rolling gait relies on the modules at both ends of the snake robot to provide friction, we applied skin to nine modules at each end of the head and tail of the snake robot. We set parameter d for the S-shaped rolling gait, hoping that there will be no contact between the middle part of the snake robot and the pipe. However, preliminary experimental results showed that due to the discrete distribution of joints, the middle part periodically contacted the pipe during the rolling process, causing the snake robot to slip on the pipe. Therefore, we assembled the housings without outer skin for the modules in the middle part to further reduce friction between the middle part and the pipe. Although the modules in the middle part cannot provide power for climbing, the shape of the modules around the pipe maintained the overall stability of the snake robot.

The diameter of both the trunk and the bifurcation in the experiment was 150 mm, and the parameter R_1 of the S-shaped curve could be obtained as 102 mm. Preliminary references for the values of parameters were provided using (27). The minimum allowable radius for all arcs in an S-shaped curve is 76.39 mm, indicating that segments 1, 2, 5, 8, and 9, which exhibit arcs or helixes will not cause joint angles to exceed this range. Setting r_1 to be greater than 115.29 mm ensures that the joint angles fitting segments 3, 4, 6, and 7 do not exceed the maximum. The parameters that determine the shape of the S-curve include D_p, d, r_1, l_5, $l_1 = l_9$ and $l_2 = l_8$, provided that the physical parameters of the snake robot remain constant. All except the diameter D_p of the pipe can be set by the operator. Since the sum of the lengths of the curve segments is limited by the total length of the snake robot, $l_2 = l_8$ is considered as the dependent variable. The parameters in the experiment were valuated according to the setup requirements and the running effect.

The action of the snake shaped robot winding the pipe required the assistance of operators. The snake robot first fitted an S-shaped curve with a diameter D_p taken as 250 mm. Then the operators supported the snake robot in surrounding the pipe. Finally, D_p was gradually reduced to 150 mm so that the snake robot was tightly wrapped around the pipe. In the experiment, the operators determined the point in time at which each step began to be executed and keyed in the relevant commands via the keyboard.

4.1. Basic climbing

We performed basic climbing motions using an S-shaped rolling gait on horizontal and vertical pipes. Considering that the mass of the snake robot during rolling was concentrated on one side of the pipe, when the pipe was horizontal, we conducted experiments on the three cases where the notch was oriented horizontally, downwardly and upwardly. Excluding the case where the pipe was horizontal and the notch was facing upwards, we set the parameters deciding the shape of the snake robot as follows: $d = 10$ mm, $l_5 = 6l$, $r_1 = 160$ mm and $l_1 = l_9 = 1.5l$. For the case where the pipe was horizontal and the notch was upward, we adjusted l_5 to $8l$ and r_1 to 150 mm so that the modules in the middle part were wrapped around the pipe to avoid dropping. Figures 16 and 17 show the experimental results of the snake robot performing basic climbing with an S-shaped rolling gait on vertical and horizontal pipes.

4.2. Overcoming bifurcation in climbing

Our primary motivation for proposing the S-shaped rolling gait is to enable the snake robot to overcome a bifurcation. We set the parameters as follows: $d = 10$ mm, $l_5 = 6l$, $r_1 = 160$ mm and $l_1 = l_9 = 1.5l$.

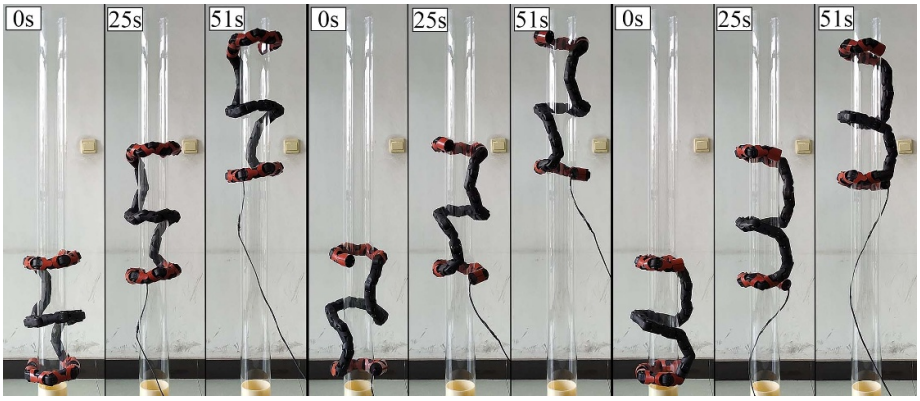

Figure 16. Experimental results of basic climbing on a vertical pipe. The views from left to right were in the order of front, back and side of the snake robot.

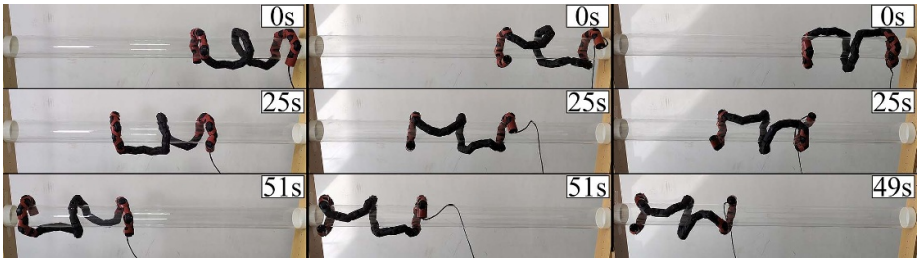

Figure 17. Experimental results of basic climbing on a horizontal pipe. The notch of the snake robot's S-shaped body faced downwards, sideways, and upwards in order from left to right.

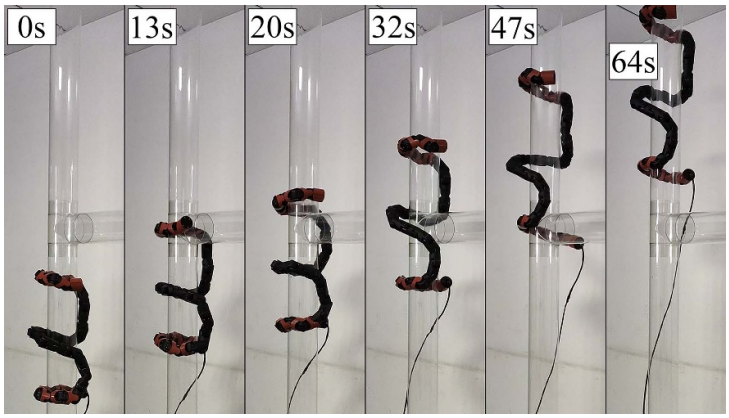

Figure 18. Experimental result of crossing a bifurcation when the trunk was vertical and the bifurcation was horizontal.

As shown in figures 18–20, when the notch of the snake robot's body and the bifurcation were in the same circumferential position, the snake robot crossed the bifurcation while rolling continuously. The snake robot underwent an extrusion with the pipe at the fork, which could be adapted due to the limited torque of the joints and the sliding between the modules and the pipe. Decreasing the values of l_5 and r_1 to increase the space available for the bifurcation did not work well. As the number of joints forming the corresponding curve segments decreased, the periodic deviation amplitude of the snake robot from the desired position increased during rolling, which reduced the stability. Unfortunately, when the trunk was horizontal and bifurcation was upwards, the snake robot could not cross the bifurcation or fall off the pipe due to gravity.

As shown in figure 21, when the notch and the bifurcation were in the opposite circumferential position, the snake robot climbed from the trunk to the bifurcation. In the process of adapting to the bifurcated shape, strong forces were generated between the snake robot and the pipe and between the internal modules. Only when the bifurcation was horizontal

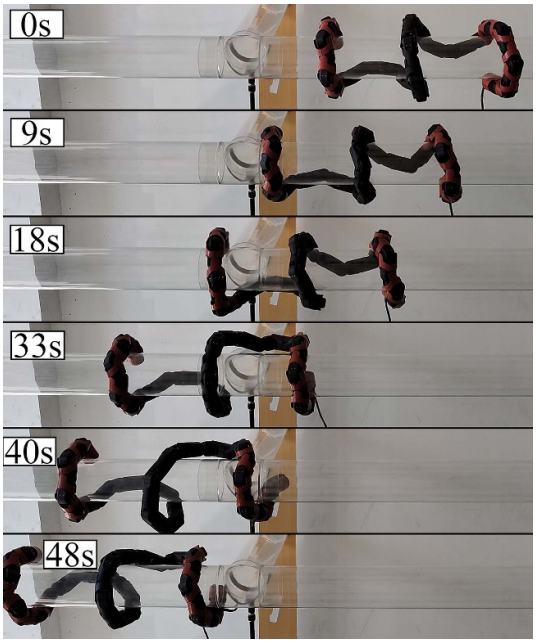

Figure 19. Experimental result of crossing a bifurcation when both the trunk and the bifurcation were horizontal.

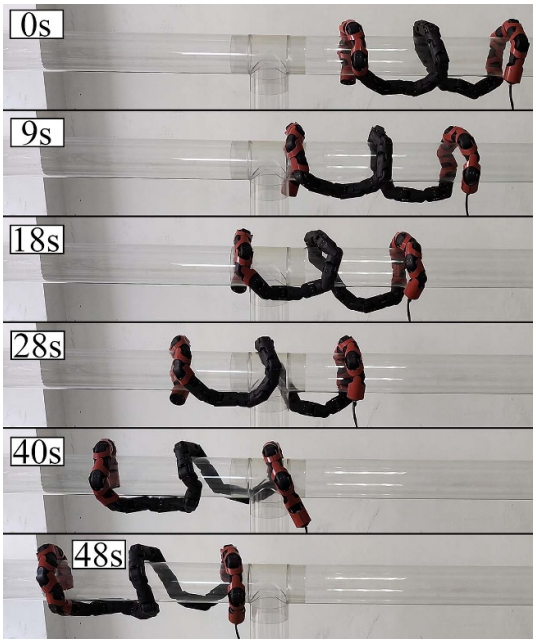

Figure 20. Experimental result of crossing a bifurcation when the trunk was horizontal and the bifurcation was downwards.

and the trunk extended upwards did the forces generated by the compliant motion balance with gravity, which ensured the stability of the snake robot on the pipe.

4.3. Circumferential rotation and adjustment

We experimentally measured the rotation velocity v_r of the snake robot with different values of β. Considering the uneven distribution of the S-shaped curve on the pipe, the pipe was placed vertically in the experiments to eliminate the influence of gravity. The experiments were performed three times for β from 0° to 7° with a step size of 1°, and the snake robot rolled for four full rounds each time. The experimental results shown in figure 22 indicate that an increase in β significantly improved the circumferential rotation velocity. Moreover, the rolling at $\beta =$ 0° demonstrated circumferential rotation, which was caused by segments 3 and 7. The larger the value of β is, the lower the stability of the gait. When β

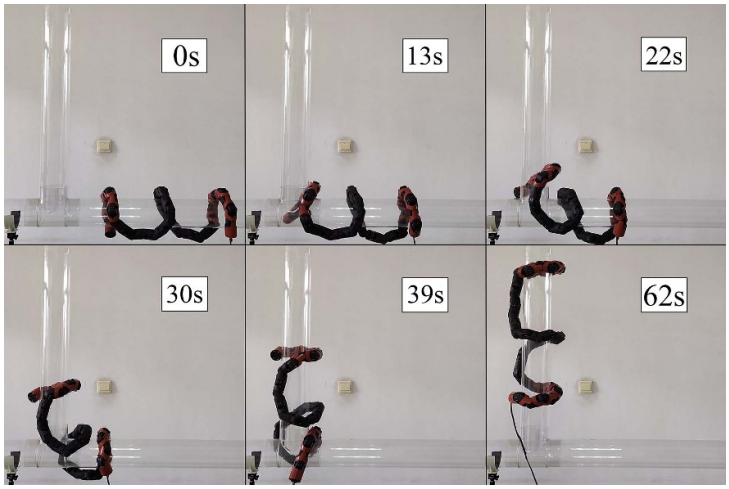

Figure 21. Experimental result of climbing to a bifurcation when the trunk was horizontal and the bifurcation was upwards.

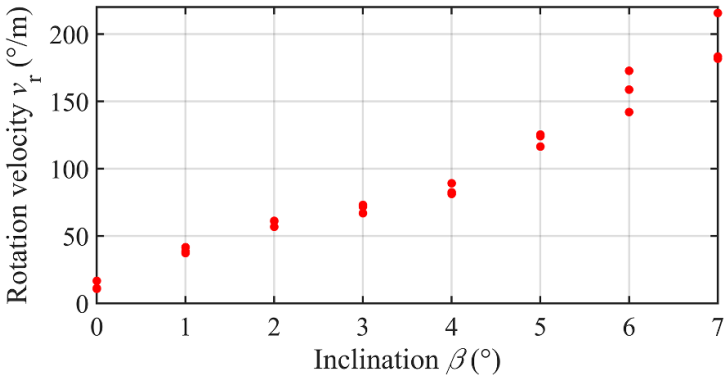

Figure 22. Experimental data of circumferential rotation velocities corresponding to different inclination angles β.

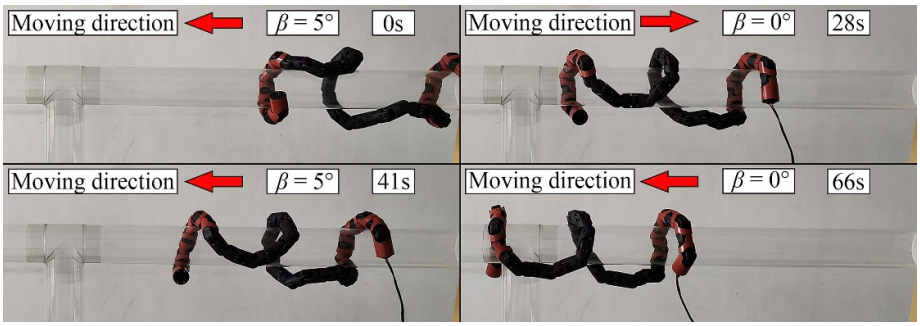

Figure 23. Experimental result of circumferential adjustment. The red arrows represent the moving directions of the snake robot.

was greater than 7°, the snake robot lost its climbing ability because it could not maintain sufficient grip force on the pipe. When the pipe was horizontal, the rotation velocities varied greatly at different circumferential positions due to gravity, but increasing β also accelerated the rotation. In addition, because the head and tail of the snake robot could track the helix well, the rotation velocity was significantly greater for the horizontal pipe than for the vertical pipe.

We sought confirm that the circumferential position of the snake robot on the pipe was adjustable using β. To demonstrate more obvious rotational motion, this experiment was thus performed with a horizontal trunk. As shown in figure 23, the initial circumferential position of the snake robot was not suitable for crossing the bifurcation and was adjusted by circumferential rotation while rolling with $\beta = 5°$. We also performed experiments on switching β on a vertical trunk to adjust the circumferential position,

but the results were not satisfactory, and the snake robot often fell off. The reason is that sudden and large changes in β caused the snake robot to shake on the pipe, and the modules located in sections 1, 2, 8 and 9 briefly detached from the pipe. Slowly varying the value of β in future studies so that the shaking is alleviated by rolling along the normal direction of the curve may solve this problem.

5. Conclusion

In this paper, we propose an S-shaped rolling gait for a snake robot designed using curve transformations, inspired by the climbing postures of biological snakes. To construct and clarify the S-shaped curve, we presented a method to establish the transformation between a planar curve and a 3D curve on a cylindrical surface. Using this method, we designed an S-shaped curve in 3D space, while analytically calculating the curvatures, torsions and twist angles in simple planar coordinate systems. With this gait, we enabled the snake robot to achieve stable climbing on the outside of a pipe. In the scenarios of forked pipes where the snake robot was able to maintain its own balance, the snake robot successfully maintained its target shapes and efficiently crossed or climbed to it the bifurcation. We also designed a form for the gait that can change the circumferential rotation velocity, and used this rotation to adjust the snake robot to the desired circumferential position on the pipe.

In the future, designing the central axis of the S-shaped curve to be controlled as straight or crooked is an important improvement, as this approach will help to address the snake robot falling off under certain conditions. In addition, realizing the transition between conventional helical and S-shaped morphologies will help the snake robot run the most appropriate climbing gait on the pipe.

Data availability statement

The data that support the findings of this study are available upon reasonable request from the authors.

Acknowledgments

This work was supported in part by the National Natural Science Foundation of China under Grants 62073328, 52274159, 62233011 and 61971423 and in part by the Natural Science Foundation of Jiangsu Province under Grant BK20200641.

Jingwen Lu's contributions to this paper were completed while he was with the School of Mechatronic Engineering, China University of Mining and Technology.

ORCID iDs

Jingwen Lu https://orcid.org/0000-0001-7415-4510
Chaoquan Tang https://orcid.org/0000-0003-1641-9845
Eryi Hu https://orcid.org/0000-0002-3932-4542
Zhipeng Li https://orcid.org/0009-0000-6529-6744

References

[1] Hirose S and Yamada H 2009 Snake-like robots [tutorial] *IEEE Robot. Autom. Mag.* **16** 88–98
[2] Lipkin K, Brown I, Peck A, Choset H, Rembisz J, Gianfortoni P and Naaktgeboren A 2007 Differentiable and piecewise differentiable gaits for snake robots *2007 IEEE/RSJ Int. Conf. Int. Conf. on Intelligent Robots and Systems* (*San Diego, CA, USA*) (IEEE) pp 1864–9
[3] Kuwada A, Wakimoto S, Suzumori K and Adomi Y 2008 Automatic pipe negotiation control for snake-like robot *2008 IEEE/ASME Int. Conf. on Advanced Intelligent Mechatronics (AIM)* (*Xian, China*) (IEEE) pp 558–63
[4] Rollinson D and Choset H 2016 Pipe network locomotion with a snake robot *J. Field Robot.* **33** 322–36
[5] Kamegawa T, Baba T and Gofuku A 2011 V-shift control for snake robot moving the inside of a pipe with helical rolling motion *2011 IEEE Int. Symp. on Safety, Security, and Rescue Robotics (SSRR)* (*Kyoto, Japan*) (IEEE) pp 1–6
[6] Inazawa M, Takemori T, Tanaka M and Matsuno F 2020 Motion design for a snake robot negotiating complicated pipe structures of a constant diameter *2020 IEEE Int. Conf. on Robotics and Automation (ICRA)* (*Paris, France*) (IEEE) pp 8073–9
[7] Inazawa M, Takemori T, Tanaka M and Matsuno F 2021 Unified approach to the motion design for a snake robot negotiating complicated pipe structures front *Robot. AI* **8** 629368
[8] Qi W, Kamegawa T and Gofuku A 2016 Proposal of helical wave propagate motion for a snake robot to across a branch on a pipe *2016 IEEE/SICE Int. Symp. on System Integration (SII)* (*Sapporo, Japan*) (IEEE) pp 821–6
[9] Qi W, Kamegawa T and Gofuku A 2017 Implementation of helical wave propagation motion in snake robot moving on exterior of a pipe *Int. J. Adv. Mechatron. Syst.* **7** 359–67
[10] Nakajima M, Cheng Q and Tanaka M 2022 Gait design and experimental validation of a snake robot on a pipe with branches using spiral stairs function *Artif. Life Robot.* **27** 300–7
[11] Takemori T, Tanaka M and Matsuno F 2023 Adaptive helical rolling of a snake robot to a straight pipe with irregular cross-sectional shape *IEEE Trans. Robot.* **39** 437–51
[12] Rollinson D and Choset H 2013 Gait-based compliant control for snake robots *2013 IEEE Int. Conf. on Robotics and Automation (ICRA)* (*Karlsruhe, Germany*) (IEEE) pp 5138–43
[13] Huang W, Guo X, Liu H and Fang Y 2023 A robust model-based radius estimation approach for helical climbing motion of snake robots *IEEE/ASME Trans. Mechatronics* **28** 3284–93
[14] Byrnes G and Jayne B C 2014 Gripping during climbing of arboreal snakes may be safe but not economical *Biol. Lett.* **10** 20140434
[15] Jayne B C, Newman S J, Zentkovich M M and Berns H M 2015 Why arboreal snakes should not be cylindrical: body shape, incline and surface roughness have interactive effects on locomotion *J. Exp. Biol.* **218** 3978–86

[16] Jayne B C 2020 What defines different modes of snake locomotion? *Integr. Comp. Biol.* **60** 156–70
[17] Savidge J A, Seibert T F, Kastner M and Jayne B C 2021 Lasso locomotion expands the climbing repertoire of snakes *Curr. Biol.* **31** R7–8
[18] Tang C, Shu X, Meng D and Zhou G 2017 Arboreal concertina locomotion of snake robots on cylinders *Int. J. Adv. Robot. Syst.* **14** 172988141774844
[19] Shu X 2018 Research on climbing gait of snake robot for truss structure *MSc Thesis* China University of Mining and Technology, China (available at: https://d.wanfangdata.com.cn/thesis/ChJUaGVzaXNOZXdTMjAyNDAxMDkSCUQwMTQ2MzE5MhoIOWR0cHh0a3c%3D)
[20] Takemori T, Tanaka M and Matsuno F 2016 Gait design of a snake robot by connecting simple shapes *2016 IEEE Int. Symp. on Safety, Security and Rescue Robotics (SSRR)* (*Lausanne*) (IEEE) pp 189–94
[21] Takemori T, Tanaka M and Matsuno F 2018 Gait design for a snake robot by connecting curve segments and experimental demonstration *IEEE Trans. Robot.* **34** 1384–91
[22] Takemori T, Tanaka M and Matsuno F 2018 Ladder climbing with a snake robot *2018 IEEE/RSJ Int. Conf. on Intelligent Robots and Systems (IROS)* (*Madrid*) (IEEE) pp 1–9
[23] Takemori T, Tanaka M and Matsuno F 2021 Hoop-passing motion for a snake robot to realize motion transition across different environments *IEEE Trans. Robot.* **37** 1696–711
[24] Konishi R, Nakajima M, Tanaka K, Matsuno F and Tanaka M 2023 Design for snake robot motion via partial grasping on pipes *Adv. Robot.* **37** 227–40
[25] Yamada H and Hirose S 2008 Study of active cord mechanism—approximations to continuous curves of a multi-joint body *J. Robot. Soc. Japan* **26** 110–20
[26] Zhen W, Gong C and Choset H 2015 Modeling rolling gaits of a snake robot *2015 IEEE Int. Conf. on Robotics and Automation (ICRA)* (*Seattle, WA, USA*) (IEEE) pp 3741–6
[27] Sun H 2007 Study on climbing snakelike robot *PhD Dissertation* Shanghai Jiao Tong University, China (available at: https://d.wanfangdata.com.cn/thesis/ChJUaGVzaXNOZXdTMjAyNDAxMDkSCFkxMjI4MjkyGgh6YTVkNXVwMw%3D%3D)